5-2008

Large Amplitude Oscillatory Shear Behavior of Entangled Polymer Solutions: Particle Tracking Velocimetric Investigation

Sham Ravindranath

Shi-Qing Wang
University of Akron Main Campus, swang@uakron.edu

Large amplitude oscillatory shear behavior of entangled polymer solutions: Particle tracking velocimetric investigation

Sham Ravindranath and Shi-Qing Wang[a)]

Department of Polymer Science and Maurice Morton Institute of Polymer Science, University of Akron, Akron, Ohio 44325

(Received 5 February 2007; final revision received 12 December 2007)

Synopsis

Large amplitude oscillatory shear (LAOS) has been employed widely to probe the nonlinear behavior of complex fluids. Typically, the system undergoing LAOS has been assumed to experience homogeneous shear in each cycle so that material functions can be introduced to analyze the nonlinear dependence of these functions on the amplitude and frequency. Using particle-tracking velocimetric technique, we have carried a more systematic investigation on four different entangled polybutadiene (PBD) solutions with the number of entanglements per chain $Z = 13$, 27, 64 and 119, extending well beyond the initial observations of shear banding in entangled PBD solutions under LAOS [Tapadia *et al.*, Phys. Rev. Lett. **96**, 196001-4 (2006a)]. At strain amplitudes $\gamma_o > 100\%$ and frequencies higher than the overall chain relaxation rate, we observed, for the three samples with 27 or more entanglements per chain, the development of a thin "liquid" layer where severe chain disentanglement may have taken place. The thin liquid layer takes most of the imposed deformation, while a significant portion of the sample stays hardly deformed and remains presumably well entangled. When the applied γ_o was between 100% and 250%, this "liquid" layer developed only after some oscillation cycles. For $\gamma_o > 300\%$, the disentangled layer formed in the first cycle, a phenomenon analogous to failure of solids under external deformation. The solution with the least entanglements of 13 per chain did not show visible inhomogeneous deformation under LAOS. © *2008 The Society of Rheology.* [DOI: 10.1122/1.2833453]

I. INTRODUCTION

Fluids possessing unique microstructures are used routinely in day to day life. They may be toothpaste, soaps, paints, lubricants, liquid crystal displays, ice cream, repellants, etc. The microstructure of these fluids provides unique properties making them suitable to a particular application. These fluids, often known as complex fluids, may be subjected to chaotic and complex flow conditions during their synthesis, processing or at the time of product usage. Thermal and deformation history alters the microstructures and thus the product properties. It is a great challenge to relate the structural changes during flow to the end properties.

The first step towards this task is to understand the microstructural changes taking place under a simple and well-defined flow deformation. This approach forms the basis of rheometry, where the response of a complex fluid subjected to a well determined defor-

[a)]Electronic mail: swang@uakron.edu

mation is characterized mechanically using force transducers. Additional methods including rheo birefringence, rheo scattering and rheo nuclear magnetic resonance have proved very valuable in detailing the structural changes during and after flow.

Oscillatory shear deformation has been an effective way to probe the complex fluids. At small amplitudes, so small that the measurement does not perturb the microstructure of a given sample, oscillatory shear experiment has provided us structural fingerprints of a variety of viscoelastic materials. With large amplitude, oscillatory shear measurements have the flexibility of varying both the frequency of oscillation and the magnitude of imposed strain with an additional advantage over continuous shear experiment: Edge effects can be minimized.

Large amplitude oscillatory shear (LAOS) protocol has been used extensively to probe gels [Knudsen *et al.* (2006)], emulsions [Mason *et al.* (1997); Bower *et al.* (1999)], surfactant solutions [Watanabe *et al.* (1982, 1997); Tirtaatmadja *et al.* (1997); Hamley *et al.* (1998); Daniel *et al.* (2001); Stangler and Abetz (2003); Hyun *et al.* (2006)], suspensions [Raghavan and Khan (1997); Yziquel *et al.* (1999); Heymann *et al.* (2002); Narumi *et al.* (2005)], yield materials [Karis *et al.* (2002a, 2003)], biopolymers [Tariq *et al.* (1998); Thien *et al.* (2000); Hyun *et al.* (2002); Veerman *et al.* (2005); Lefebvre (2006)], electrorheological and magnetorheological fluids [Parthasarathy and Klingenberg (1999); Sim *et al.* (2003a); Hu *et al.* (2006)], filled polymers [Krishnamoorti and Giannelis (1997, 2001); Ren *et al.* (2000, 2003)], polymer solutions and melts [Adrian and Giacomin (1992); Reimers and Dealy (1996); Wilhelm (2002), Debbaut and Burhin (2002); Clemeur *et al.* (2003); Schlatter *et al.* (2005)].

In most cases, LAOS produces a nonsinusoidal stress response, i.e., distorted sine waves for a variety of materials under examination. This means that the material in question is no longer able to respond in a linear manner to the applied sinusoidal strain. As subharmonic frequencies emerge, the material functions such as G' and G'' no longer have any meaning. Considerable efforts have been made towards obtaining useful and desirable material information from LAOS experiments. Graphical representations such as Lissajous curves have been employed to describe the nonlinear response. Interpretation in terms of Fourier analysis has been suggested. Notably, Wilhelm *et al.* have extensively applied Fourier analysis for LAOS in different systems [Wilhelm *et al.* (1998, 1999, 2000); Dusschoten *et al.* (2001); Kallus *et al.* (2001); Neidhofer *et al.* (2003, 2004)]. Fourier analysis has also been employed by Karis *et al.* (2002b) and Sim *et al.* (2003b) in their papers. Cho *et al.* (2005) have proposed a new method of interpretation based on the geometric aspect of viscoelasticity. Here, the material properties in the nonlinear regime are extracted by means of generalized storage modulus and generalized loss modulus. LAOS results have also been compared with network model [Yosick *et al.* (1996, 1997); Sim *et al.* (2003b)], separable Berstein, Kearsley and Zapas (BKZ) model [Giacomin *et al.* (1993)] and molecular stress function model [Wapperom *et al.* (2005)], in an attempt to relate the results to underlying physics. These efforts formed a theoretical background concerning the origin of the observed nonlinear behavior under LAOS, in hope that LAOS measurements could become fingerprints detailing inherent material properties.

More recently, using an effective particle-tracking velocimetry technique (PTV), Tapadia, Ravindranath and Wang (2006a) have reported the first revelation of shear banding in entangled polybutadiene solutions under LAOS. They suggested that the inhomogeneous shear is due to uneven development of disentanglement across the gap, when a frequency higher than the overall chain relaxation rate was applied. Since disentanglement is a kind of structural rearrangement, the observed shear banding in entangled polybutadiene solutions hints at the possibility of similar banding in other complex or structured fluids. The coexistence of different local shear rates across the sample thick-

TABLE I. Molecular characteristics of long chain PBDs.

Sample	M_n (g/mol)	M_w (g/mol)	M_w/M_n	Source
700 K	0.74×10^6	0.75×10^6	1.02	Bridgestone
1.0 M	1.014×10^6	1.052×10^6	1.03	University of Akron
1.8 M	1.56×10^6	1.86×10^6	1.19	Goodyear

ness appears to be responsible for the observed nonsinusoidal stress response. If a sample is not undergoing homogeneous shear during LAOS as in the case of entangled polymer solutions, it would not be valid anymore to analyze the time dependence of the measured shear stress and cast the information in terms of any material functions.

Ongoing research activities in our group have revealed banding under LAOS in other complex fluids including aqueous DNA solutions and micellar solutions. In this report, we focus on describing the rheological and PTV observations of monodisperse polybutadiene solutions with the number of entanglements per chain Z ranging from 13 to 119. Except for the sample with $Z=13$, others show somehow similar behavior, and therefore we only need to report more extensively on the sample with $Z=64$.

II. EXPERIMENTAL SECTION

A. Materials

The molecular characteristics of high molecular weight 1,4-polybutadiene (PBD) and short chain oligomeric polybutadiene can be found in Tables I and II, respectively. Entangled 1,4-polybutadiene solutions were prepared by dissolving different weight% of high molecular weight PBD in oligomeric PBD. The samples were prepared by first dissolving high molecular weight PBDs in toluene to which low molecular weight oligomeric PBD was added. Silver-coated particles with an average diameter of 10 μm (Dantec Dynamics HGS-10) were first ultrasonicated in toluene and then added to the solution. The final loading of the particles was at a level of 200–600 ppm. Toluene was allowed to evaporate at room temperature for nearly a week under hood. Residual toluene was completely removed under vacuum for about 48 h; 700 K(5%)–1.8 K sample refers to 5 wt% of 700 K PBD dissolved in 1.8 K oligomeric PBD. Similarly, the other three solutions are labeled as 700 K(10%)–3.8 K, 1.0 M(15%)–9 K and 1.8 M(15%) –3.8 K. These four samples have the number of entanglements per chain Z given by 13, 27, 64 and 119, respectively, where the last solution is slightly polydisperse. Small amplitude oscillatory shear measurements indicate the terminal relaxation times of 42, 8 and 67 s for the first three solutions, respectively. Thus, the Rouse relaxation time τ_R can be estimated to be 3.2, 0.3 and 1 s, respectively.

TABLE II. Molecular characteristics of short chain oligomeric PBDs.

Sample	M_n (g/mol)	M_w (g/mol)	M_w/M_n	Source
1.8 K	1800	⋯	⋯	Sigma-Aldrich *Cat. No. 20,043-3*
3.8 K	3500	3800	1.08	Goodyear
9 K	8500	8900	1.04	Goodyear

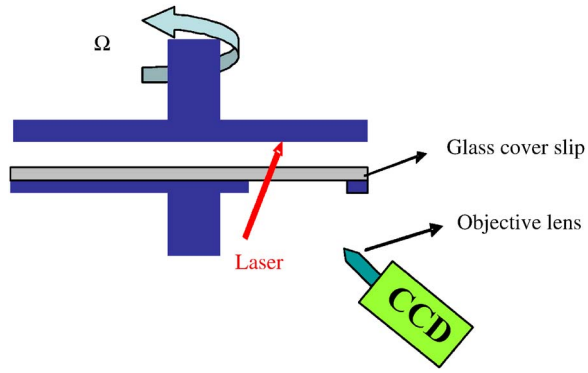

FIG. 1. Particle-tracking velocimetry setup, where the upper rotating plate is made of steel. Lower stationary steel plate with a hole is covered with a glass cover slip, so that silver particles in the sample can be illuminated with a laser and watched with a CCD camera placed at an angle.

B. Apparatus and data representation

LAOS experiments in displacement mode were carried out on a stress-controlled Bohlin-CVOR rheometer at room temperature that can perform large amplitude oscillatory shear (LAOS) and give output of both strain and stress signals as a function of time for each cycle during LAOS. Like any other rotational rheometers, the Bohlin-CVOR does not have proper software to analyze nonlinear responses including distortion of the sinusoidal waves. Despite the distortion and generation of subharmonics, the instrument still gives an amplitude for the measured shear stress σ_o, G' and G''. Although their meanings cannot be explicitly defined, these three quantities still give an averaged representation of the viscoelasticity during LAOS. We will use them below without being more rigorous. Because of this approximate depiction, we also tolerate the fact that in a parallel-plate setup the total angular displacement and total torque do not directly correspond to the strain and shear stress experienced by the entire sample, where there is a radial distribution of strain amplitudes and corresponding stress values. 1.0 M(15%) −9 K and 1.8 M(15%)−3.8 K entangled solutions were tested on 25-mm-diam parallel-plate disks, while 700 K(5%)−1.8 K and 700 K(10%)−3.8 K solutions were tested on 35 mm diameter parallel-plate disks. Advanced Rheometrics Expansion System was used for small amplitude oscillatory-shear (SAOS) frequency sweep measurements at room temperature.

C. Particle-tracking velocimetry setup (PTV)

In this work, a laser sheet with a cross section of 0.2 mm × 2 mm is passed across the gap at an angle to illuminate the sliver particles embedded in the sample. During shearing, movement of the illuminated particles across the entire sample thickness is videotaped using a black-white charge coupled device (CCD) camera (with a maximum speed of 30 frames per second). Figure 1 shows the schematic setup. The CCD camera is mounted with a DIN objective lens (3.2X) through an adaptive tube (Edmund Optics: U54-868). During analysis, distance traveled by a particle can be determined by playing 1–3 frames using MGI Videowave 4 software. By adopting the technique of passing laser sheet at an angle ~45° through the stationary plate, the velocity profile at different radial distances from the center can be easily determined by just changing the location of the laser sheet. In case of 1.0 M(15%)−9 K and 1.8 M(15%)−3.8 K solutions, PTV obser-

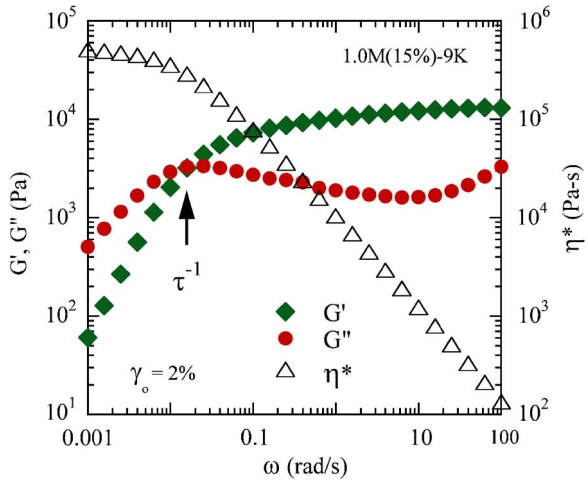

FIG. 2. Dynamic storage modulus G', loss modulus G'' and complex viscosity $|\eta^*|$ of 1.0 M[15%]−9 K solution from oscillatory shear measurements using a strain amplitude of 2% at room temperature around 25 °C.

vations were made at a radial distance 4 mm from the edge in a 25-mm-diam parallel-plate shear cell, while for 700 K(5%)−1.8 K and 700 K(10%)−3.8 K solutions observations were made at a radial distance 8 mm from the edge in 35-mm-diam parallel-plate disks. Note that in all cases we specify the strain amplitude as that at the location of the PTV observation.

III. RESULTS AND DISCUSSION

A. Banding through chain orientation and diffusion

Since the frequencies applied in LAOS experiments are chosen based on the information of linear viscoelasticity of these samples, SAOS measurement was first carried out on 1.0 M(15%)−9 K entangled solution at room temperature. Figure 2 shows the crossover frequency $\omega_c = \tau^{-1}$ to be around 0.015 rad/s. Except in the following Sec. III C, we will focus on exploring the various aspects of LAOS of this sample. So unless specified, all figures below are results of our study on this sample.

For a given oscillating frequency ω and strain amplitude γ_o, the entangled network would undergo a maximum shear rate of $\dot{\gamma} = \gamma_o \omega$. To probe the nonlinear behavior of entangled solutions, frequencies ω greater than crossover frequency ω_c were employed in all of our LAOS experiments. At frequencies $\omega > \omega_c$, the rate of shear deformation is faster than the overall rate of chain relaxation, insuring that the chains would orient in the flow direction.

The 1.0 M(15%)−9 K entangled solution showed linear response under oscillatory shear deformation of $\gamma_o = 70\%$, over the range of frequencies tested, from 0.1 to 16 rad/s, i.e., Lissajous plots (shear stress vs. shear strain loop) were perfectly "elliptical." Our PTV observations indicate that the shear deformation was homogeneous at $\gamma_o = 70\%$ for all the frequencies tested.

The apparent viscoelastic functions at $\gamma_o = 100\%$ and $\omega = 1$ rad/s are shown in Fig. 3. Unlike the behavior at $\gamma_o = 70\%$, the elastic modulus G' and shear stress proportional to $|G^*|$ decreases within a few oscillating cycles, while the value of viscous modulus G'' increases. Under the influence of this LAOS, the entangled chains apparently were able to

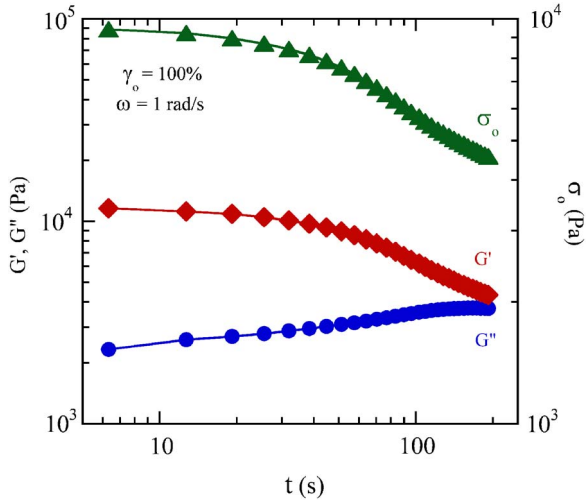

FIG. 3. Rheological response of 1.0 M(15%)−9 K solution at room temperature for an oscillatory shear deformation of strain amplitude γ_o=100% and frequency ω=1 rad/s > ω_c; 25 mm parallel-plate disks were used and the strain amplitude γ_o=100% is at the radial distance of 4 mm from the edge.

orient sufficiently and arrange themselves into a new environment with reduced topological hindrance to each other, resulting in a decrease of G'. At the end, G' and G'' are almost equal. It is likely that this is a state of less chain entanglement. Lissajous plots presented in Fig. 4 provide a useful picture of the response of the entangled network. In Fig. 4, undistorted ellipse can be noticed at 62 s, while distorted ellipse can be seen at 125 s and beyond. It seems the entanglement network was able to self-organize into a state of less entanglement in a uniform manner before displaying a nonlinear response.

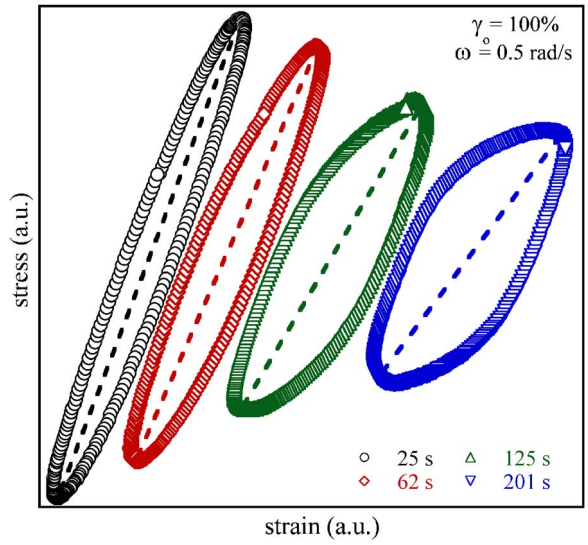

FIG. 4. Lissajous plots of 1.0 M(15%)−9 K solution at different times for an oscillatory shear deformation of strain amplitude γ_o=100% and frequency ω=0.5 rad/s > ω_c. Lissajous plot is obtained by plotting stress voltage signal vs. strain voltage signal in arbitrary units.

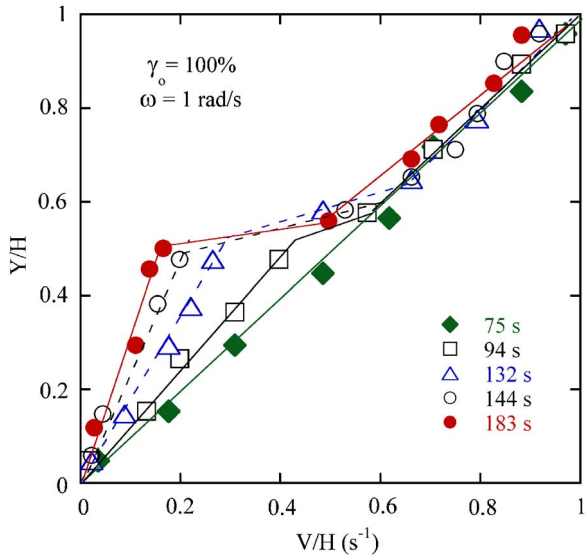

FIG. 5. Velocity profiles at the instant of maximum plate speed for different times at a radial distance of 4 mm from the edge in 25 mm parallel-plate disks. The sample at this radial distance experienced 100% strain amplitude and the applied frequency was 1 rad/s.

PTV observations of this LAOS offered surprising insight into the shift from linear to nonlinear response. The velocity profile across the sample thickness at the instant of maximum plate speed at a radial distance of 4 mm from the edge is shown in Fig. 5. Figure 5 portrays linear velocity profile up to 75 s. Then a striking banding emerges by 94 s. With time the entangled network evolves into regions of three different shear rates, with most of the imposed deformation taken by the thinnest fluid layer in the center of the sample where the local shear rate is the highest. After 150 s, very little evolution of banding takes place and steady state velocity profile is represented by solid circles in Fig. 5. The local shear rates at this moment in the lower solid region, middle fluid layer and upper region are ~0.3, 5.5 and 1.2 s^{-1}, respectively, indicating that the ″liquid″ layer experiences a shear rate 18 times higher than that of the "solid" region. Note that the averaged shear rate is $\gamma_o\omega = 1.0\ s^{-1}$. Apparently, the entangled network could not undergo uniform shear in steady state. After sufficient reorganization of their entanglement states during the induction period where no banding was observed, an anisotropic condition was eventually met to allow more dramatic disentanglement that evidently refused to take place uniformly across the sample thickness. For this sample, strain amplitude $\gamma_o = 100\%$ is the necessary condition to produce enough chain deformation for banding to take place. Unlike the observations of Tapadia *et al.* (2006a) on polydisperse samples, where the thickness of the fluid layer gradually grows with time, the fluid layer in our monodisperse sample does not grow in its thickness but instead evolves into higher and higher shear rate values while the solid layers settle to lower rates.

The velocity profile for different frequencies $\omega > \omega_c$ at $\gamma_o = 100\%$ and at the instant of maximum plate speed is presented in Fig. 6. Independent of the applied frequency, banding was first observed at ~90 s, which is slightly more than the reptation time τ indicated in Fig. 1. Since ω varied by a factor of 4, for a given time duration the sample experienced four times as many cycles at $\omega = 2$ rad/s as it had at $\omega = 0.5$ rad/s. It is remarkable that the emergence of banding occurs at the same time. Figure 7 shows the

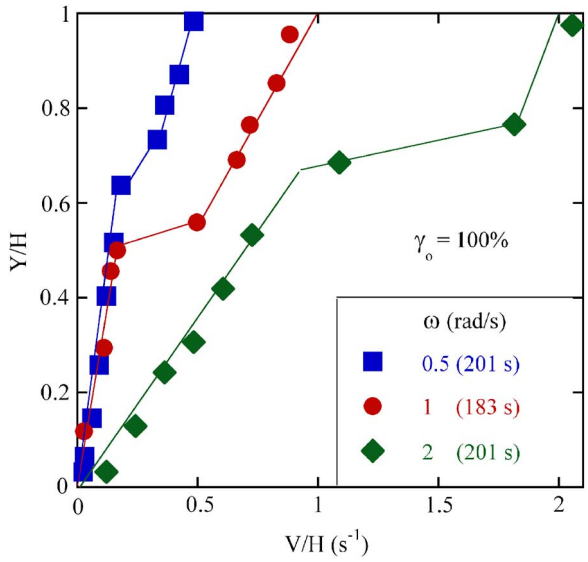

FIG. 6. Velocity profiles at the instant of maximum plate speed for different oscillating frequencies at a radial distance of 4 mm from the edge in 25 mm parallel-plate disks. The sample at this radial distance experienced 100% strain amplitude.

variations in banding at the instants of 3/8th and 5/8th of an oscillating cycle corresponding to the same plate speed. At these long times the system has reached "steady state," i.e., the velocity profiles are the same in every subsequent cycle.

Similar banding features were observed when strain amplitude was increased to 125%. At γ_o=125%, banding was first observed at ~60 s independent of the range of frequen-

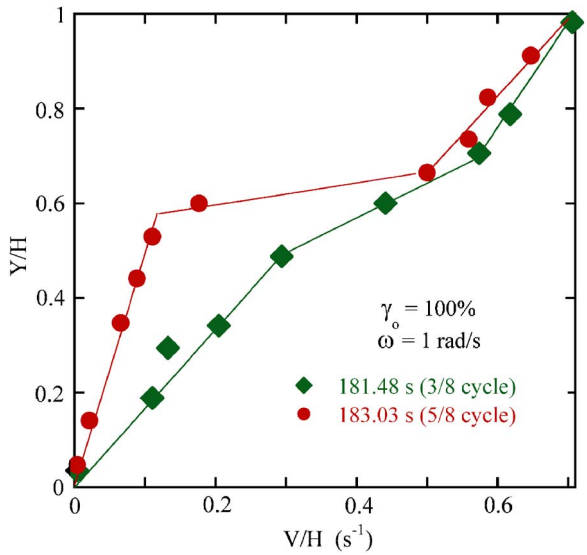

FIG. 7. Velocity profiles show the variation in banding at the instants of 3/8th and 5/8th of an oscillating cycle that have the same plate speed (but lower than maximum value). The sample at this radial distance experienced 100% strain amplitude and the applied frequency was 1 rad/s.

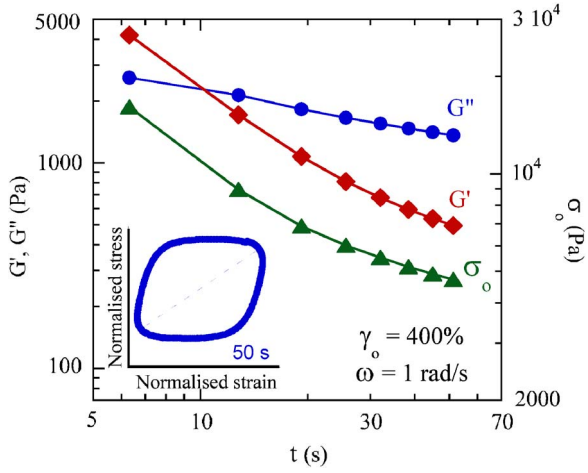

FIG. 8. Rheological response of 1.0 M(15%)−9 K solution at room temperature for an oscillatory shear deformation of strain amplitude γ_o=400% and frequency ω=1 rad/s>ω_c. The strain amplitude γ_o=400% is at the radial distance of 4 mm from the edge. The inset shows the Lissajous plot at 50 s.

cies $\omega > \omega_c$ investigated (0.5–4 rad/s). Even at γ_o=125%, it takes 60 s of shearing before banding takes place. At γ_o=250%, banding could be observed after ~20 s of oscillatory shearing. As the applied strain amplitude γ_o increases to produce higher chain orientation and deformation, the time taken to display banding diminishes.

B. Banding due to catastrophic yielding

Unlike the behavior at strain amplitudes $\gamma_o < 250\%$, where nonlinear response is observed only after some oscillation cycles, the response is highly nonlinear even within the first oscillatory cycle at strain amplitudes $\gamma_o > 300\%$. Figure 8 shows rheological responses in terms of the apparent mechanical signals and Lissajous plot for γ_o=400% and frequency ω=1 rad/s. Experiments at amplitudes γ_o=400% were terminated at 65 s, well before any noticeable edge fracture could take place. From the distorted ellipse, a highly nonlinear velocity profile can be expected. Figure 9 shows the evolution of the banding profiles with time at the instant of the maximum plate speed. By completion of the 6th cycle (37.68 s), little change in banding profile takes place and the steady state profile is represented by solid circles in Fig. 9.

The local shear rates in the lower solid region, middle fluid layer and upper region are ~0.75, 16 and 4.5 s^{-1}, respectively, whereas the averaged shear rate is $\gamma_o\omega$=4.0 s^{-1}. The steady state velocity profiles at the maximum plate speed at γ_o=400% for different oscillating frequencies are plotted in Fig. 10. Even at frequency as low as 0.1 rad/s, which is just six times higher than the crossover frequency ω_c, i.e., $\omega\tau_R < Z$, banding developed within the first cycle. Figure 11 shows the banding profile at this frequency at 197 s.

Clearly, at $\gamma_o > 300\%$, the banding occurs almost immediately. It is evident that sufficient chain deformation has produced enough elastic retraction force F_{retract} in each entangled chain. This force F_{retract} can overcome the cohesion of the entanglement network [Wang *et al.* (2007)]. Here F_{retract} is simply proportional to the amplitude γ_o since $\sigma = |G^*|\gamma_o$.

It is important to point out that the banding profiles are random and irreproducible. Since a well-rested sample is initially uniform across its thickness, banding locations are

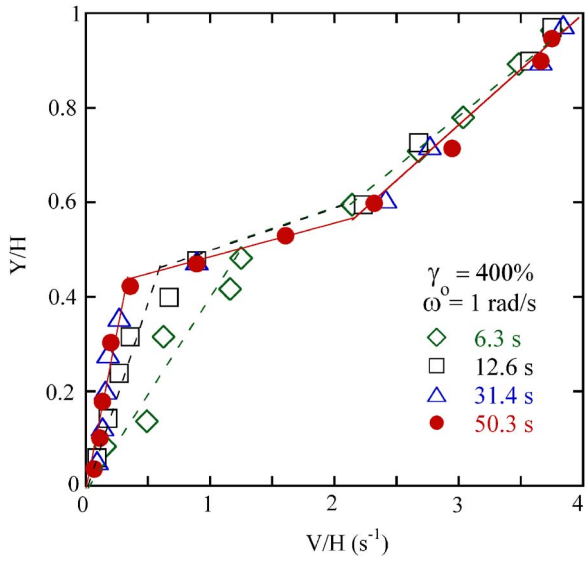

FIG. 9. Velocity profiles at different times at the instant of maximum plate speed at a radial distance of 4 mm from the edge in 25 mm parallel-plate disks. The sample at this radial distance experienced 400% strain amplitude and the applied frequency was 1 rad/s.

arbitrary. The velocity profiles of two identical tests at γ_o=275% and ω=1 rad/s are shown in Fig. 12. Here more than one band was observed in each test, showing the different positions of the "liquid" layers. Though the locations of bands varied, the rheological responses in the inset of Fig. 12 for the two tests show the same behavior.

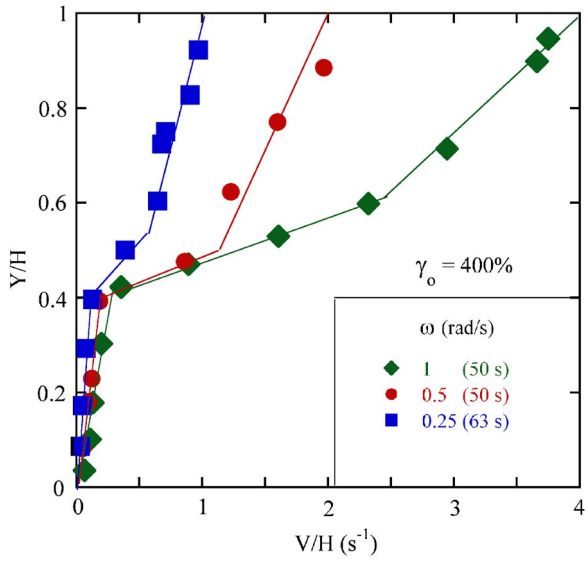

FIG. 10. Velocity profiles at different oscillating frequencies for a strain amplitude of 400% at the instant of maximum plate speed.

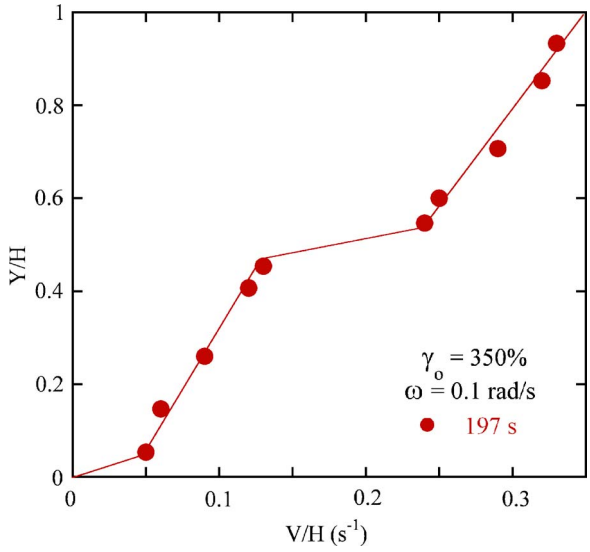

FIG. 11. Velocity profile at the instant of maximum plate speed at a radial distance of 4 mm from the edge in 25 mm parallel-plate disks. The sample at this radial distance experienced 350% strain amplitude and the applied frequency was 0.1 rad/s.

C. Effect of entanglement level

Three other entangled polybutadiene solutions 700 K(5%)−1.8 K, 700 K(10%) −3.8 K and 1.8 M(15%)−3.8 K were also studied to see how their LAOS behavior varies with the degree of chain entanglement. These samples have the number Z of entanglements per chain varying from 13, 27 to 119.

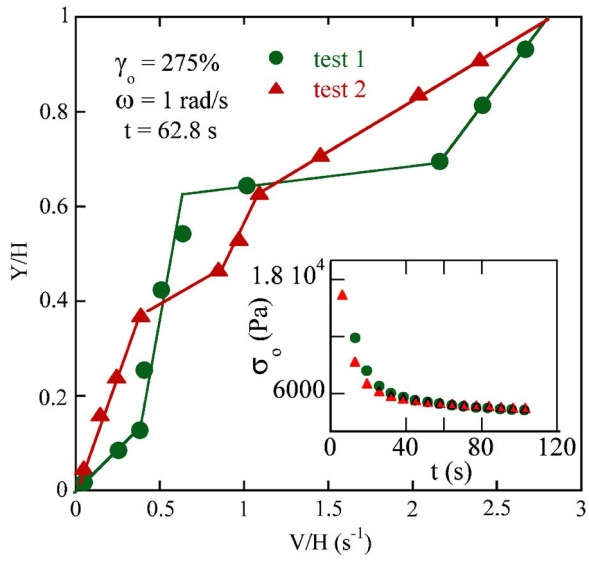

FIG. 12. Velocity profiles for two repeats at the instant of maximum plate speed at a radial distance of 4 mm from the edge in 25 mm parallel-plate disks. For both the repeats, the sample at this radial distance experienced 275% strain amplitude and the frequency was 1 rad/s. The inset shows the rheological response of the solution for the two repeats.

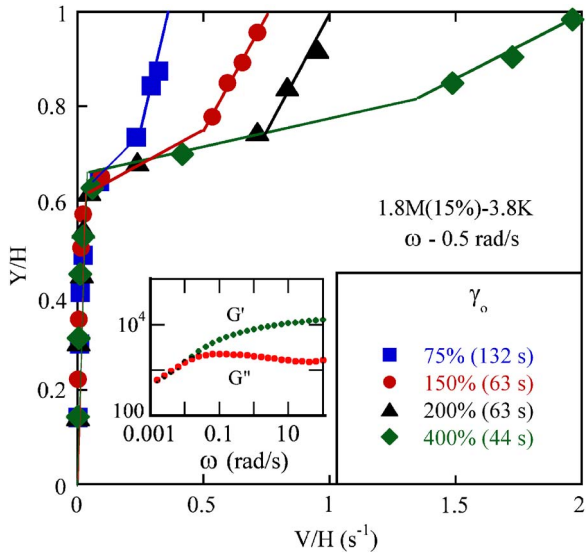

FIG. 13. Velocity profiles of 1.8 M(15%)−3.8 K solution at different strain amplitudes for an oscillating frequency of 0.5 rad/s at the instant of maximum plate speed. The profiles were observed at a radial distance of 4 mm from the edge in 25 mm parallel-plate disks. The inset shows the storage modulus G′ and loss modulus G″ of the solution from oscillatory shear measurements using a strain amplitude of 2% at 25 °C.

As in 1.0 M(15%)−9 K entangled solution, LAOS experiments on 1.8 M(15%) −3.8 K were done using 25 mm parallel-plate disks and PTV observations at a radial position 4 mm from the edge. Figure 13 shows the steady state velocity profiles at the maximum plate speed at ω=0.5 rad/s for different strain amplitudes γ_o. Since this sample is twice as entangled as that studied in the preceding Secs. III A and III B, banding was much stronger and could be first observed at strain amplitude γ_o=75%. For all the amplitudes, the entangled solid-like layer hardly experiences any deformation. The ratio of local shear rates in the entangled to disentangled layer at γ_o=400% was as high as 9/0.15=60 in contrast to a factor of 20 in 1.0 M(15%)−9 K. Apart from this, all other features are similar to the sample investigated in the preceding subsections.

The least entangled solution 700 K(5%)−1.8 K solution with Z=13 entanglement points per chain and τ=42 s only shows a linear velocity profile at oscillating frequency of 0.25 rad/s and γ_o=900%, where a flexible film was wrapped around the meniscus to prevent the possible occurrence of edge fracture at such large strain amplitudes. Though the velocity profile was linear at all times, the stress response was nonsinusoidal as indicated in a Lissajous plot. It is presently unclear whether the film at the meniscus caused a nonlinear response in LAOS.

When the level of entanglements per chain was increased to 27, shear banding could be observed again under LAOS. To compare with results on the 700 K(5%)−1.8 K solution, 35 mm parallel-plate disks were used and a flexible film was wrapped around the meniscus. Figure 14 shows the velocity profiles at the maximum plate speed at a radial distance of 8 mm from the edge for different frequencies at strain amplitude γ_o =400%. At frequencies ω=1 and 2 rad/s, two liquid layers could be observed by the end of the first cycle. The nonlinearity in velocity profile was weaker when ω=0.5 rad/s was used, which is just five times the crossover frequency ω_c. Nevertheless, for entangled network with degree of entanglements greater than 25, banding can be observed at frequency $\omega > 5\omega_c$ and at strain amplitudes $\gamma_o > 100\%$.

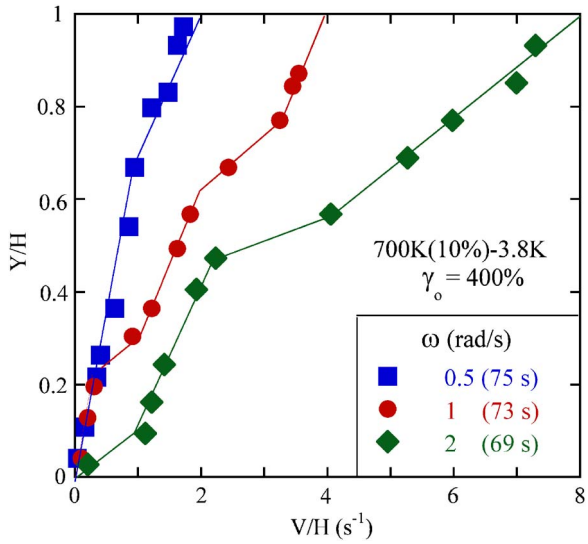

FIG. 14. Velocity profiles of 700 K(10%)−3.8 K solution for different oscillating frequencies at the instant of maximum plate speed at a radial distance of 8 mm from the edge in 35 mm parallel-plate disks. Sample at this radial distance experienced 400% strain amplitude.

D. Summary

We may summarize our PTV observations of LAOS in entangled polymer solutions in terms of a diagram to highlight the significant difference, with which the system develop nonuniform deformation. Figure 15 shows that shear banding may occur via two different mechanisms, i.e., either because of an elastic breakdown of the entanglement network at

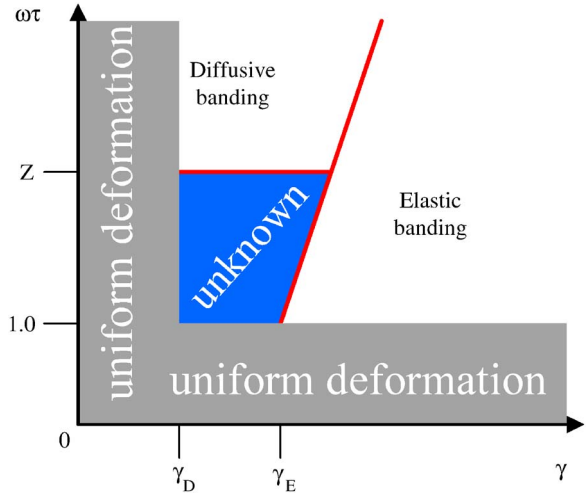

FIG. 15. "Phase diagram" depicting the various conditions, under which banding occurs through two different mechanisms, where $\omega\tau=Z$ is the same condition as $\omega\tau_R=1$, $\gamma_D\approx 0.8$ and $\gamma_E\approx 2.7$. No experimental information is currently available in the middle region although it is tempting to think that this middle region is also part of the "diffusive banding" region.

high enough strains or due to rearrangement of the state of chain entanglement over a time scale comparable to the dominant chain diffusion time τ. For simplicity, we call them elastic banding and diffusive banding, respectively.

IV. CONCLUSION

Nonlinear flow behavior of entangled polybutadiene solutions with different degrees of chain entanglement has been investigated under LAOS using a rheo-PTV technique. In this report, we have shown coexistence of multiple shear rates under LAOS across the sample thickness in entangled solutions with $Z > 25$. This finding shed new light on previous studies that used LAOS to characterize entangled polymers and other viscoelastic materials. In contrast to those earlier PTV observations on the polydisperse solution [Tapadia *et al.* (2006a)], we find in the present *monodisperse* solutions that at strain amplitudes γ_o between 100% and 250%, nonlinear velocity profile is seen only after some oscillating cycles. In other words, at these levels of chain deformation, the entangled chains may first reorganize into a less entangled state through diffusion of these deformed chains and then disentangle inhomogeneously to produce shear banding. In the Lissajous plots, distortion of an ellipse begins to appear when nonlinear velocity profile is first noticed. At strain amplitudes $\gamma_o > 300\%$, liquid-like layer of less entanglement developed instantaneously, i.e., within the first cycle of oscillation. This behavior is well anticipated when new theoretical considerations are taken into account as provided recently [Wang *et al.* (2007)]. As long as the conditions of $\gamma_o > 100\%$ and $\omega > \omega_c$ are met, banding would form, where the thickness of the liquid layer hardly changes although the local shear rate in such a layer may rise over time until the steady state is reached. In some instances more than one band formed across the gap. Even though highly distorted ellipses are seen in Lissajous plots of the entangled solution with $Z = 13$, the velocity profile is linear at all times.

All of the reported features under LAOS are consistent with characteristics of the same samples undergoing startup shear [Tapadia and Wang (2006b); Boukany and Wang (2007); Ravindranath *et al.* (2007a)] and step shear [Wang *et al.* (2006); Ravindranath and Wang (2007b)]. The commonality is inhomogeneous shear response to imposed external boundary condition. Phenomenologically, the nonuniformity must correspond to different states of chain entanglement in the different layers across the sample thickness. These experimental observations have prompted us to put forward a new theoretical framework [Wang *et al.* (2007)] within which to better understand the rich variety of flow phenomena in entangled polymer solutions and melts. Specifically, when large deformation is imposed on a time scale much shorter than the dominant chain relaxation time τ, the entanglement network breaks down as any solid of finite cohesive strength would do. The cohesion of entangled polymers on time scales much shorter than τ is due to chain entanglement. The observed nonuniformity is therefore plausibly due to chain disentanglement that can occur either because of an elastic breakup of the entanglement network or because of adjustment of the chain entanglement by molecular diffusion in presence of modest shear oscillations.

ACKNOWLEDGMENTS

This work is supported, in part, by a Small Grant for Exploratory Research of the National Science Foundation (DMR-0603951) and an ACS grant (PRF No. 40596-AC7).

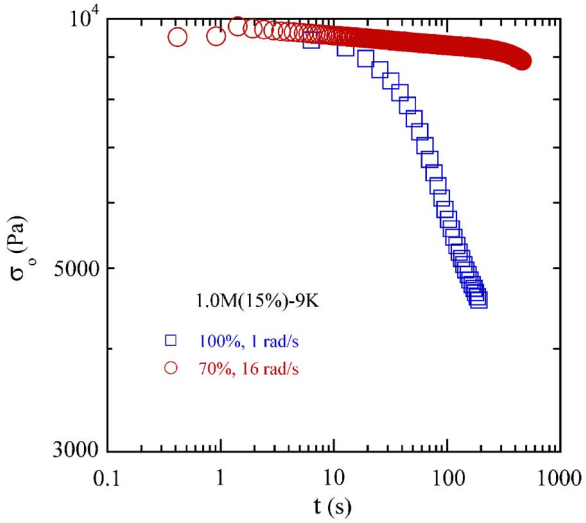

FIG. 16. Stress responses of 1.0 M(15%)−9 K solution to LAOS of γ_o=70%, ω=16 rad/s and γ_o=100%, ω=1 rad/s.

APPENDIX A: VISCOUS HEATING

The rate of viscous heat produced during flow can be estimated by $\sigma\dot{\gamma}$, where σ is the stress generated in the sample and $\dot{\gamma}$ is the applied shear rate. In thermal equilibrium, such a rate of heat generation is conducted away from the sample into the shear cell according to $\kappa(T_s-T_{pl})/(H/2)^2$, i.e., we have

$$\sigma\dot{\gamma} \sim 4\kappa(T_s - T_{pl})/H^2, \tag{A1}$$

where κ is the thermal conductivity coefficient for the polymer, T_s is the final sample temperature in the middle of the gap and T_{pl} the plate temperature, $H/2$ is the traveling distance of thermal conduction, on the order of half the sample thickness H. For a shear stress peak as high as 10 KPa at an effective shear rate of $\omega\gamma_o \sim 1\ s^{-1}$, we have T_s-T_{pl} $\sim 0.025\ ^\circ$C, where we use κ=0.1 W/m °C and H=1 mm. For the viscosity to change by a factor of 2 due to a temperature change there must be a temperature change of 20 °C, a thousand times higher than our estimate.

Figure 16 compares the stress response of 1.0 M(15%)−9 K solution to LAOS of γ_o=70%, ω=16 rad/s and γ_o=100%, ω=1 rad/s. From Fig. 16, it can be noticed that at all times the stress generated in the sample at γ_o=70% and ω=16 rad/s is higher than that at γ_o=100% and ω=1 rad/s. But shear banding is not observed in the case of γ_o =70% and ω=16 rad/s even when sheared for 500 s, while nonlinear velocity profile is observed for γ_o=100% and ω=1 rad/s as shown in Fig. 5.

APPENDIX B: BANDING IN CONE AND PLATE GEOMETRY

All the banding features observed in parallel-plate disks can be similarly observed in a cone-plate setup. We employed a parallel-plate setup to avoid the presence of any stress gradient along the gap that could be interpreted by some as the origin of shear banding. It is helpful and instructive to also carry out similar PTV measurements in a cone-plate shear cell. In Fig. 17 the banding features of the 1.0 M(15%)−9 K solutions under LAOS deformation of γ_o=350% for different frequencies are presented, where a cone-

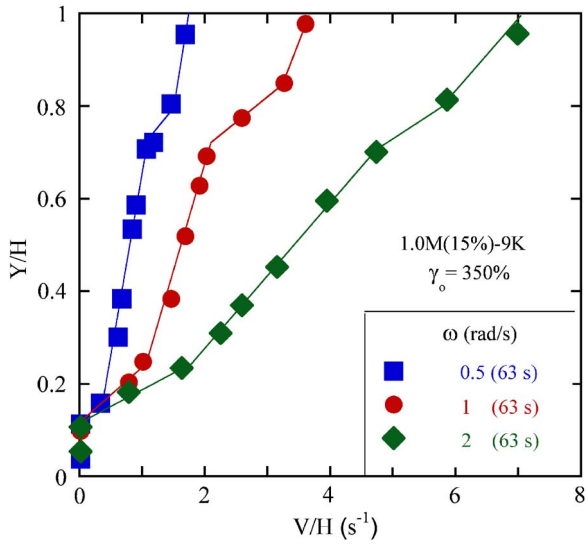

FIG. 17. Velocity profiles of the 1.0 M(15%)−9 K sample for different oscillating frequencies at the instant of maximum plate speed at a radial distance of 4 mm from the edge in 25 mm/50° cone-plate disks. Sample at this radial distance experienced 350% strain amplitude.

plate assembly with diameter 25 mm and cone angle equal to 5° was used. Although only steady state profiles were presented, a fluid-like layer was also found to develop within the first cycle.

References

Adrian, D. W., and A. J. Giacomin, "The quasi-periodic nature of a polyurethane melt in oscillatory shear," J. Rheol. **36**, 1227–1243 (1992).

Boukany, P. E., and S. Q. Wang, "A correlation between velocity profile and molecular weight distribution in sheared entangled polymer solutions," J. Rheol. **51**, 217–233 (2007).

Bower, C., C. Gallegos, M. R. Mackley, and J. M. Madiedo, "The rheological and microstructural characterization of the non-linear flow behavior of concentrated oil-in-water emulsions," Rheol. Acta **38**, 145–159 (1999).

Cho, K. S., K. Hyun, K. H. Ahn, and S. J. Lee, "A geometrical interpretation of large amplitude oscillatory shear response," J. Rheol. **49**, 747–758 (2005).

Clemeur, N., R. P. G. Rutgers, and B. Debbaut, "On the evaluation of some differential formulations for the pom-pom constitutive model," Rheol. Acta **42**, 217–231 (2003).

Daniel, C., I. W. Hamley, M. Wilhelm, and W. Mingvanish, "Non-linear rheology of a face-centered cubic phase in a diblock copolymer gel," Rheol. Acta **40**, 39–48 (2001).

Debbaut, B., and H. Burhin, "Large amplitude oscillatory shear and Fourier-transform rheology for a high-density polyethylene: Experiments and numerical simulation," J. Rheol. **46**, 1155–1176 (2002).

Dusschoten, D. V., M. Wilhelm, and H. W. Spiess, "Two-dimensional Fourier transform rheology," J. Rheol. **45**, 1319–1339 (2001).

Giacomin, A. J., R. S. Jeyaseelan, T. Samurkas, and J. M. Dealy, "Validity of separable BKZ model for large amplitude oscillatory shear," J. Rheol. **37**, 811–826 (1993).

Hamley, I. W., J. A. Pople, C. Booth, L. Derici, M. I. Clerc, and P. Davidson, "Shear-induced orientation of the body-centered-cubic phase in a diblock copolymer gel," Phys. Rev. E **58**(6), 7620–7628 (1998).

Heymann, L., S. Peukert, and N. Aksel, "Investigation of the solid-liquid transition of highly concentrated suspensions in oscillatory amplitude sweeps," J. Rheol. **46**, 93–112 (2002).

Hu, B., A. Fuchs, S. Huseyin, F. Gordaninejad, and C. Evrensel, "Supramolecular magnetorheological polymer gels," J. Appl. Polym. Sci. **100**, 2464–2479 (2006).

Hyun, K., S. H. Kim, K. H. Ahn, and S. J. Lee, "Large amplitude oscillatory shear as a way to classify the complex fluids," J. Non-Newtonian Fluid Mech. **107**, 51–65 (2002).

Hyun, K., J. G. Nam, M. Wilhelm, K. H. Ahn, and S. J. Lee, "Large amplitude oscillatory shear behavior of PEO-PPO-PEO triblock copolymer solutions," Rheol. Acta **45**, 239–249 (2006).

Kallus, S., N. Willenbacher, S. Kirsch, D. Distler, T. Neidhofer, M. Wilhelm, and H. W. Spiess, "Characterization of polymer dispersions by Fourier transform rheology," Rheol. Acta **40**, 552–559 (2001).

Karis, T. E., C. A. Kim, and M. S. Jhon, "Harmonic analysis of a solder paste under large amplitude oscillatory shear," Macromol. Mater. Eng. **287**, 583–587 (2002a).

Karis, T. E., C. M. Seymour, R. N. Kono, and M. S. Jhon, "Harmonic analysis in rheological property measurement," Rheol. Acta **41**, 471–474 (2002b).

Karis, T. E., R. N. Kono, and M. S. Jhon, "Harmonic analysis in grease rheology," J. Appl. Polym. Sci. **90**, 334–343 (2003).

Knudsen, J. C., A. O. Karlsson, R. Ipsen, and L. H. Skibsted, "Rheology of stirred acidified skim milk gels with different particle interactions," Colloids Surf., A **274**, 56–61 (2006).

Krishnamoorti, R., and E. P. Giannelis, "Rheology of end-tethered polymer layered silicate nanocomposites," Macromolecules **30**, 4097–4102 (1997).

Krishnamoorti, R., and E. P. Giannelis, "Strain hardening in model polymer brushes under Shear," Langmuir **17**, 1448–1452 (2001).

Lefebvre, J., "An outline of the non-linear viscoelastic behavior of wheat flour dough in shear," Rheol. Acta **45**, 525–538 (2006).

Mason, T. G., M. D. Lacasse, G. S. Grest, D. Levine, J. Bibette, and D. A. Weitz, "Osmotic pressure and viscoelastic shear moduli of concentrated emulsions," Phys. Rev. E **56**(3), 3150–3166 (1997).

Narumi, T., H. See, A. Suzuki, and T. Hasegawa, "Response of concentrated suspensions under large amplitude oscillatory shear flow," J. Rheol. **49**, 71–85 (2005).

Neidhofer, T., M. Wilhelm, and B. Debbuat, "Fourier-transform rheology experiments and finite-element simulations on linear polystyrene solutions," J. Rheol. **47**, 1351–1371 (2003).

Neidhofer, T., S. Sioula, N. Hadjichristidis, and M. Wilhelm, "Distinguishing linear from star-branched polystyrene solutions with Fourier-transform rheology," Macromol. Rapid Commun. **25**, 1921–1926 (2004).

Parthasarathy, M., and D. J. Klingenberg, "Large amplitude oscillatory shear of ER suspensions," J. Non-Newtonian Fluid Mech. **81**, 83–104 (1999).

Raghavan, S. R., and S. A. Khan, "Shear-thickening response of fumed silica suspensions under steady and oscillatory shear," J. Colloid Interface Sci. **185**, 57–67 (1997).

Ravindranath, S., S. Q. Wang, M. Olechnowicz, and R. P. Quirk, "Shear banding in steady state during startup shear of entangled polymer solutions," Macromolecules, under review (2007a).

Ravindranath, S., and S. Q. Wang, "What are the origins of stress relaxation behaviors in step shear of entangled polymer solutions?," Macromolecules **40**, 8031–8039 (2007b).

Reimers, M. J., and J. M. Dealy, "Sliding plate rheometer studies of concentrated polystyrene solutions: Large amplitude oscillatory shear of a very high molecular weight polymer in diethyl Phthalate," J. Rheol. **40**, 167–186 (1996).

Ren, J., A. S. Silva, and R. Krishnamoorti, "Linear viscoelasticity of disordered polystyrene-polyisoprene block copolymer based layered-silicate nanocomposites," Macromolecules **33**, 3739–3746 (2000).

Ren, J., B. F. Casanueva, C. A. Mitchell, and R. Krishnamoorti, "Disorientation kinetics of aligned polymer layered silicate nanocomposites," Macromolecules **36**, 4188–4194 (2003).

Schlatter, G., G. Fleury, and R. Muller, "Fourier transform rheology of branched polyethylene: Experiments and models for assessing the macromolecular architecture," Macromolecules **38**, 6492–6503 (2005).

Sim, H. G., K. H. Ahn, and S. J. Lee, "Three-dimensional dynamics simulation of electrorheological fluids under large amplitude oscillatory shear flow," J. Rheol. **47**, 879–895 (2003a).

Sim, H. G., K. H. Ahn, and S. J. Lee, "Large amplitude oscillatory shear behavior of complex fluids investi-

gated by a network model: A guideline for classification," J. Non-Newtonian Fluid Mech. **112**, 237–250 (2003b).

Stangler, S., and V. Abetz, "Orientation behavior of AB and ABC block copolymers under large amplitude oscillatory shear flow," Rheol. Acta **42**, 569–577 (2003).

Tapadia, P., S. Ravindranath, and S. Q. Wang, "Banding in entangled polymer fluids under oscillatory shearing," Phys. Rev. Lett. **96**, 196001 (2006a).

Tapadia, P., and S. Q. Wang, "Direct visualization of continuous simple shear in non-Newtonian polymeric fluids," Phys. Rev. Lett. **96**, 016001 (2006b).

Tariq, S., A. J. Giacomin, and S. Gunasekaran, "Nonlinear viscoelasticity of cheese," Biorheology **35**, 171–191 (1998).

Thien, N. P., M. Newberry, and R. I. Tanner, "Non-linear oscillatory flow of a soft solid-like viscoelastic material," J. Non-Newtonian Fluid Mech. **92**, 67–80 (2000).

Tirtaatmadja, V., K. C. Tam, and R. D. Jenkins, "Superposition of oscillations on steady shear flow as a technique for investigating the structure of associative polymers," Macromolecules **30**, 1426–1433 (1997).

Veerman, C., L. M. C. Sagis, P. Venema, and E. V. D. Linden, "Shear-induced aggregation and break up of fibril clusters close to the percolation concentration," Rheol. Acta **44**, 244–249 (2005).

Wang, S. Q., S. Ravindranath, P. Boukany, M. Olechnowicz, R. Quirk, A. Halasa, and J. Mays, "Non-quiescent relaxation of entangled polymeric liquids after step strain," Phys. Rev. Lett. **97**, 187801 (2006).

Wang, S. Q., S. Ravindranath, Y. Wang, and P. Boukany, "New theoretical considerations in polymer rheology: Elastic breakdown of chain entanglement network," J. Chem. Phys. **127**, 064903-14 (2007).

Wapperom, P., A. Leygue, and R. Keunings, "Numerical simulation of large amplitude oscillatory shear of a high-density polyethylene melt using the MSF model," J. Non-Newtonian Fluid Mech. **130**, 63–76 (2005).

Watanabe, H., T. Kotaka, T. Hashimoto, M. Shibayama, and H. Kawai, "Rheological and morphological behavior of styrene-butadiene diblock copolymer solutions in selective solvents," J. Rheol. **26**, 153–179 (1982).

Watanabe, H., T. Sato, K. Osaki, M. L. Yao, and A. Yamagishi, "Rheological and dielectric behavior of a styrene-isoprene-styrene triblock copolymer in selective solvents. 2. Contribution of loop-type middle blocks to elasticity and plasticity," Macromolecules **30**, 5877–5892 (1997).

Wilhelm, M., D. Maring, and H. W. Spiess, "Fourier-transform rheology," Rheol. Acta **37**, 399–405 (1998).

Wilhelm, M., P. Reinheimer, and M. Ortseifer, "High sensitivity Fourier-transform rheology," Rheol. Acta **38**, 349–356 (1999).

Wilhelm, M., P. Reinheimer, M. Ortseifer, T. Neidhofer, and H. W. Spiess, "The crossover between linear and non-linear mechanical behavior in polymer solutions as detected by Fourier-transfrom rheology," Rheol. Acta **39**, 241–246 (2000).

Wilhelm, M., "Fourier-transform rheology," Macromol. Mater. Eng. **287**, 83–105 (2002).

Yosick, J. A., and A. J. Giacomin, "Can nonlinear deformation amplify subtle differences in linear viscoelasticity," J. Non-Newtonian Fluid Mech. **66**, 193–212 (1996).

Yosick, J. A., A. J. Giacomin, and P. Moldenaers, "A kinetic network model for nonlinear flow behavior of molten plastics in both shear and extension," J. Non-Newtonian Fluid Mech. **70**, 103–123 (1997).

Yziquel, F., P. J. Carreau, and P. A. Tanguy, "Non-linear viscoelastic behavior of fumed silica suspensions," Rheol. Acta **38**, 14–25 (1999).